Spherical supershells in metal clusters and the transition to protocrystalline structure

Keith Clemenger*
Institute of Physics, Chinese Academy of Sciences, P.O. Box 603, Beijing 100080, China
(Received 9 July 1991)

One-electron calculations of spherical supershell structure are presented for metal clusters with up to 8000 valence electrons over the range of metallic densities $2 \leq r_s \leq 6$, using potentials adapted from self-consistent bulk surface calculations. Good agreement is obtained with detailed trends in the experimental data and with corresponding self-consistent cluster jellium calculations throughout. In the $T=0$ limit, aspherical perturbations anticipated from the incipient ionic lattice are shown to eradicate the supershell structure at a cluster size corresponding to near-degeneracy at the Fermi level between valence-electron states differing by $\Delta l=4$, where l is the angular-momentum quantum number. This critical size is on the order of $N \sim 10^3$ valence electrons for all metallic densities; in the specific case $r_s=4$, the result is $N=1640$, in excellent agreement with the experimentally observed transition in Na clusters to "shells of atoms" in the range $1400 < N < 2000$.

I. INTRODUCTION

Electronic shell structure has been observed in atomic clusters of a wide variety of metals, including the alkali and noble metals, and such diverse polyvalent metals as Al and Pb.[1–7] This shell structure is analogous to the shell structures found in atomic and nuclear physics, with the valence electrons of the metal highly delocalized, and bound to first approximation within a spherical effective potential. The most common experimental evidence for shell structure has been the observation of abundance variations in mass spectra, but specific physical properties of clusters have also been investigated, including photoionization potentials, static polarizabilities, and collective dipole resonances. In each case, shell effects have been observed.

These studies were conducted on small clusters, typically with less than 100 atoms. More recently, spherical shell effects have been observed in mass spectra of Na and Cs metal clusters containing several hundred atoms.[8,9] The experimentally observed pattern of features corresponds to the sequence of the largest theoretically predicted energy gaps between electron shells. For still larger Na clusters, mass spectra show a distinctly different pattern of abundance variations above 1500 atoms.[10] In the region Na_n, $1500 < n < 22\,000$, the pattern is associated not with electronic shells, but with icosahedral or cuboctahedral "shells of atoms."

Stimulated by the promise of spherical shell structure in systems with hundreds or even thousands of electrons, there has been a renewal of theoretical interest in eigenvalue density oscillations, or "bunching" of eigenvalues, in cavities small enough that the ratio of the wavelength to the dimensions of the cavity is not a very small quantity.[11–13] Although the fundamental theory is, strictly speaking, restricted to cavities with infinitesimal boundaries, the density oscillations also occur for models with more complex potential shapes. This has recently been demonstrated for Woods-Saxon and "wine-bottle" potential shapes more nearly characteristic of clusters.[13] In a metal cluster, the maxima in the eigenvalue density oscillations correspond to groups of electron shells which lie close together in energy. Following Ref. 13, we refer to these groups of shells as "supershells."

An appropriate choice of fitting parameters for the Woods-Saxon potential[13] gives good agreement with experiment for Na clusters up to several hundred atoms.[9] This success of the model makes it attractive to extend it to other metals, and to larger clusters. Results from the two phenomenological potentials studied in Ref. 13 show significant differences, however; it is hard to know which potential shape would give more accurate results, particularly as the number of valence electrons increases.

The present paper examines the dependence of the electron energy level distribution on the details of the radial potential. In Sec. II, a simple model is employed to investigate trends in supershell patterns among different metallic densities, and to illustrate the special need for accuracy in the potential shape close to the cluster surface. Section III presents detailed numerical calculations of supershell effects for the entire range of metallic densities using effective spherical potential shapes adapted from a self-consistent study of flat metal surfaces;[14] comparison of these results with experiment is emphasized. Section IV goes on to investigate the implications of spherical supershell models for aspherical structural transitions such as those recently observed in Na clusters of thousands of atoms. Section V presents a summary of our conclusions.

II. GENERAL SCALING ARGUMENTS

The following definitions are adopted throughout. We will always mean by N the number of valence electrons in the cluster; $a_0=\hbar^2/me^2$ is the Bohr radius; the Wigner-Seitz radius r_s is defined by $4\pi(a_0 r_s)^3/3=1/n_0$, n_0 being the valence-electron density in the bulk metal; and $R_0=a_0 r_s N^{1/3}$ is a characteristic cluster radius.[15]

In this section, a simple model is developed which will illustrate some basic features of the dependence of supershell patterns on metallic density. We begin with an observation about the Schrödinger equation with a spherically symmetric potential $V(r)$: any linear change of radial and energy scales which leaves the product $V(r)r^2$ invariant results in the same equation. The energy eigenvalue distribution (i.e., the supershell structure) is precisely the same, apart from the scaling of the energy variable, for problems which transform in this way.

Consider the variations in effective one-particle metal cluster potentials $V(r)$ as a function of the parameter r_s. A natural set of units for free-electron-gas problems expresses length in units of the Fermi wavelength λ_F, and energy in units of the Fermi energy ε_F:

$$k_F=\left[\frac{9\pi}{4}\right]^{1/3}(a_0 r_s)^{-1}\ ,$$
$$\lambda_F=2\pi/k_F\ , \tag{2.1}$$
$$\varepsilon_F=\frac{\hbar^2 k_F^2}{2m}\ .$$

To the extent that the set of potential functions $V(r)$ for various metals scale in energy as ε_F and in length as λ_F, the product $V(r)r^2$ is independent of k_F, and thus independent of r_s. For such an idealized set of potential wells, the supershell structure is the same for all metallic densities.

We consider the energy scale first. Bulk surface calculations[14] suggest values for the depth of the cluster potential well in the range $1.3\varepsilon_F$ (for $r_s=2$) to $2.7\varepsilon_F$ (for $r_s=6$). This moderate variation with r_s might be expected to lead to changes in the supershell structure; the direct effect, however, is negligible. This is so because supershells, being a semiclassical property of bound states, essentially depend only on the shape of the potential below the highest occupied state (here, the Fermi level); the shape of the well above the Fermi level is irrelevant to the problem in the semiclassical limit.[16]

A simple potential form appropriate to the present problem may therefore be constructed as follows. We describe the shape of the potential beneath the Fermi level with a Woods-Saxon parametrization, fixing the well depth so that the potential at the cluster radius R_0 corresponds to the Fermi level. The total depth of the Woods-Saxon potential well then becomes fixed at $2\varepsilon_F$, regardless of the metal:

$$V(r)=\frac{-2\varepsilon_F}{1+\exp[(r-R_0)/\alpha]}\ . \tag{2.2}$$

The parameter α characterizes the length over which the potential varies significantly near R_0. Transforming to dimensionless (starred) variables by dividing all lengths by λ_F and all energies by ε_F, we arrive at the scaled form

$$V^*(r^*)=\frac{-2}{1+\exp[(r^*-R_0^*)/\alpha^*]}\ , \tag{2.3a}$$

$$R_0^*=R_0/\lambda_F=\left[\frac{9N}{32\pi^2}\right]^{1/3}=0.3054N^{1/3}\ , \tag{2.3b}$$

independent of r_s, with the possible exception of $\alpha^*=\alpha/\lambda_F$.

The surface width coefficient α^* may be estimated[17] by considering the surface correction term in the expression for the density of eigenvalues in a cavity[11]

$$\rho(k)=\frac{\Omega k^2}{2\pi^2}\mp\frac{Sk}{8\pi}+O(R/\Omega)\ , \tag{2.4}$$

where Ω, S, and R are the volume, surface area, and radius of the cavity, and the minus and plus signs denote Dirichlet and Neumann boundary conditions, respectively. The total number of electrons N in a spherical volume of radius R is given by an integral over the density of states (including a spin degeneracy of 2) up to the Fermi level. Neglecting terms of order R/Ω,

$$N=2\int_0^{k_F}\rho(k)dk=\frac{4}{9\pi}(k_F R)^3\mp\tfrac{1}{2}(k_F R)^2\ . \tag{2.5}$$

For a fixed number of electrons N the radii R_D and R_N corresponding to Dirichlet and Neumann boundary conditions will differ, but they will be related by the above constraint:

$$\frac{4}{9\pi}(k_F R_D)^3-\tfrac{1}{2}(k_F R_D)^2=\frac{4}{9\pi}(k_F R_N)^3+\tfrac{1}{2}(k_F R_N)^2\ . \tag{2.6}$$

For purposes of estimation, we may take the radius R_D of the Dirichlet problem to indicate the point at which the electron density falls effectively to zero, and the radius R_N of the Neumann problem to indicate the point at which the electron density reaches its maximum inside the cluster. Then the first-order difference w of these two radii

$$w=R_D-R_N\simeq\frac{3\pi}{4k_F}=\tfrac{3}{8}\lambda_F \tag{2.7}$$

is a measure of the width over which the electron charge density varies at the surface. Now spatial variations in the electron density near the surface closely correspond to variations in the one-electron potential; so we also take w to be an estimate of the width over which the potential varies at the cluster surface.

This width, along with the actual cluster potential depth U, leads to a first-order estimate U/w of the slope of the potential at the cluster surface; in dimensionless form, $8U^*/3$, where $U^*=U/\varepsilon_F$ and $\lambda_F^*=1$. Associating this slope with the slope $1/2\alpha^*$ of the Woods-Saxon potential (2.3) at R_0^*, we find the general relationship

$$U^*\alpha^*=\tfrac{3}{16}=0.1875\ . \tag{2.8}$$

In this simple model, if U^* is constant, so is α^*, and supershell patterns are invariant. However, as U^* increases, α^* decreases, sharpening the potential edge and causing the well to be deeper just inside the surface. As a result, states of higher angular momentum l tend to be

lowered in energy relative to surrounding states, and "bunching" or near degeneracy of levels differing in l by 3,4,5,6,. . . occurs at smaller values of N. Supershell patterns shift to smaller N for a sharper potential edge.

The general result (2.8) may be compared with the parameters adopted in Ref. 13 based on comparison with self-consistent calculations for Na clusters:

$$U^*\alpha^* = \frac{U}{\varepsilon_F}\frac{\alpha}{\lambda_F} = \frac{6.0\text{ eV}}{3.24\text{ eV}}\frac{0.74\text{ Å}}{6.81\text{ Å}} = 0.201\ . \quad (2.9)$$

The model may also be applied to atomic nuclei; average estimates from the nuclear physics literature[18] for the various quantities give

$$U^*\alpha^* = \frac{U}{\varepsilon_F}\frac{\alpha}{\lambda_F} = \frac{50\text{ MeV}}{37\text{ MeV}}\frac{0.67\ fm}{4.62\ fm} = 0.196\ . \quad (2.10)$$

Results for both clusters and nuclei are thus in very reasonable agreement with the present model.

Sharpening of the potential well at the cluster surface is only one of a variety of changes which may cause variations in the supershell structure. Chief among the remaining effects is the variation in the potential shape just inside the cluster surface. The previous analysis indicates that for typical values, $\alpha \ll \lambda_F$. In such a potential, the semiclassical electron orbits (those with relatively high angular momentum) will, like their classical counterparts, be largely confined to the first Fermi wavelength inside the surface. These states will depend sensitively on the detailed potential shape in that region, and variations in the one-particle potential shape near the surface, such as those associated with Friedel oscillations, will significantly influence the energies of these states, i.e., their supershell structure.

In summary, we expect the supershell patterns for metal clusters to vary only moderately with r_s, but the variations which are expected depend strongly on the potential just inside the surface. The calculations of Sec. III will therefore be devised to emphasize careful treatment of the surface region.

III. NUMERICAL CALCULATIONS

Given the large number and size of clusters to be considered in this study, we choose to model the effective one-particle potential of a cluster by taking over the corresponding potentials from published self-consistent local-density-approximation (LDA) calculations of flat metal surfaces, with the radial coordinate r substituted for the Cartesian coordinate x.

There are several advantages to this approach. It is simple: calculation of all energy eigenvalues for each of thousands of clusters can be performed on a microcomputer. Although no recursive techniques are used to achieve self-consistency, the potentials adopted are based directly on the potentials of a self-consistent theory of the bulk metal surface. It is thus an approximation particularly suited to studies of large clusters; it should improve in accuracy as the number of valence electrons N increases toward the bulk limit. Moreover, a range of potentials are available, each corresponding to a specific electron density, so that varying results can be correlated with the variations in electron density among different metals. Finally, the present method gives a detailed description of the potential just inside the cluster surface.

Potentials from self-consistent LDA calculations of metal clusters[19,20] and bulk surfaces[14] are very similar near the surface, even for very small clusters. Near the center the cluster LDA potentials vary significantly with N, alternately rising or falling at $r=0$ to satisfy the requirements of self-consistency. The present approach makes no attempt to achieve self-consistency, and so does not describe these details. However, the good correspondence between cluster and bulk potentials near the surface should lead to calculations which do approximately reflect the supershell patterns of much more complicated self-consistent cluster calculations. This approximation should become even better in the limit of large N, and it retains the distinctive features caused by Friedel oscillations near the surface.

The published potentials of Lang and Kohn (LK) (Ref. 14) are adopted in the present study. To model the cluster potentials, we fix the jellium edge $x=0$ of the LK potentials at the radius $r=R_0$, and potentials are truncated at a distance R_0 in from this edge at the center of the cluster ($r=0$). For the larger clusters, where the radial extent exceeds the range of values given by LK, the po-

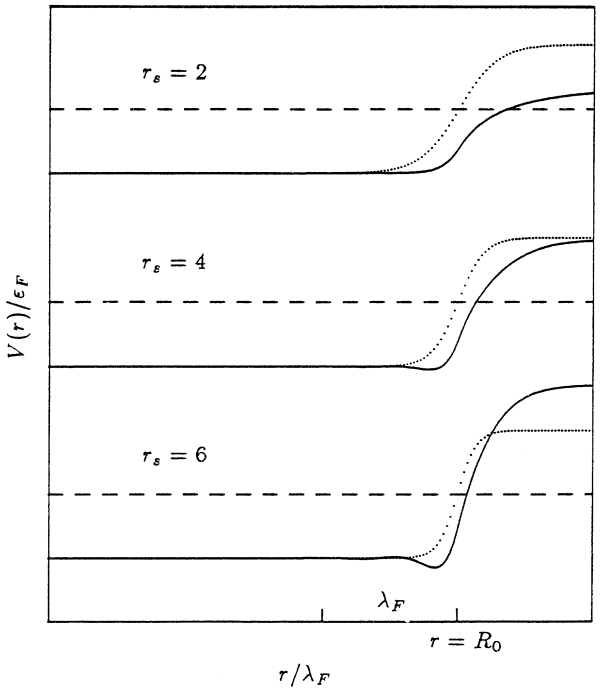

FIG. 1. Effective metal cluster potentials, in dimensionless form, for $N=1000$. Solid lines: potentials used in the present study (adapted from Ref. 14). Dashed lines: the Fermi level. Dotted lines: Woods-Saxon potentials (2.3); α^* is determined in each case from (2.8), with U^* taken from the LK potential depth.

tentials are extended inward to $r=0$ at the constant value of the potential far within the metal.[21]

Potentials for $r_s=2$, 4, 6 are displayed in Fig. 1 along with corresponding Woods-Saxon potentials from the analysis of Sec. II. The approximate scaling of the adapted LK potentials with ε_F and λ_F is evident, but certain features of the potential wells vary substantially with r_s, particularly in the region just inside the surface. The variation with r_s of the potential slope at the surface is well described by the analysis of Sec. II. Features which differ from that analysis include the shift of the potential wall beyond R_0 corresponding to spillout of the electron gas at the surface, and oscillations in the effective potential corresponding to Friedel oscillations in the electron density. When allowance is made for the outward shift of the potential wall, the $r_s=2$ potential in the critical region just inside the surface looks very much like the Woods-Saxon case. As r_s increases, the potentials deepen inside the surface from the Friedel oscillations. Just as the sharpening of the potential wall shifts the supershell pattern by lowering the high-l states, so too this deepening of the potential in the surface region will shift the supershell patterns to smaller N.

In principle, the proposed substitution of the radial coordinate r for the Cartesian coordinate x is a reliable approximation only when the cluster radius is much greater than the characteristic width of the cluster surface; in terms of the Woods-Saxon potential, $R_0^* \gg \alpha^*$, or roughly $N^{1/3} \gg 0.3$. This condition is well satisfied for all but the very smallest clusters. Performance of the model for the smallest clusters will be discussed below when comparison is made with experiment.

A. Results

Calculations of energy levels were performed using the Wentzel-Kramers-Brillouin (WKB) approximation[22] for a selection of cluster sizes in the range $1 \le N \le 8000$. The selection was made by increasing $N^{1/3}$ successively in increments of 0.04, and selecting the nearest integer N for calculation. To ensure that the clusters with closed shells were included, the value of N corresponding to filling of the topmost (partially filled) electron shell was retained during the course of each calculation. Calculations were performed for each of these values of N also.

To make comparisons with experiment, we follow Ref. 13 and calculate a "shell energy"

$$E_{\text{shell}}(N)=E(N)-E_{\text{av}}(N)\ , \tag{3.1a}$$

$$E(N)=\sum_{i=1}^{N}\varepsilon_i\ , \tag{3.1b}$$

where ε_i are the one-particle energies of the N valence electrons measured from the bottom of the potential well,[21] and $E_{\text{av}}(N)$ is determined by a parametrized fit to the set of points $E(N)$ for a series of clusters. In this work we make a least-squares fit to an expansion in powers of $N^{1/3}$, resulting in the equation

$$E_{\text{av}}(N)=\varepsilon_F(a_v N+a_s N^{2/3}+a_c N^{1/3}+a_d)\ . \tag{3.2}$$

Values of the coefficients, and a discussion of their physical significance, are given in Appendix A. The volume coefficient a_v is found in each case to be very close to the bulk free-electron-gas value $a_v=\frac{3}{5}$, as it should be. The other coefficients depend sensitively on surface properties. For the purposes of the present analysis, $E_{\text{av}}(N)$ simply provides a convenient means for isolating the shell effects.

$E_{\text{shell}}(N)$ is displayed in Fig. 2 for integral values of r_s. A calculation of an infinite square well of radius R_0 is in-

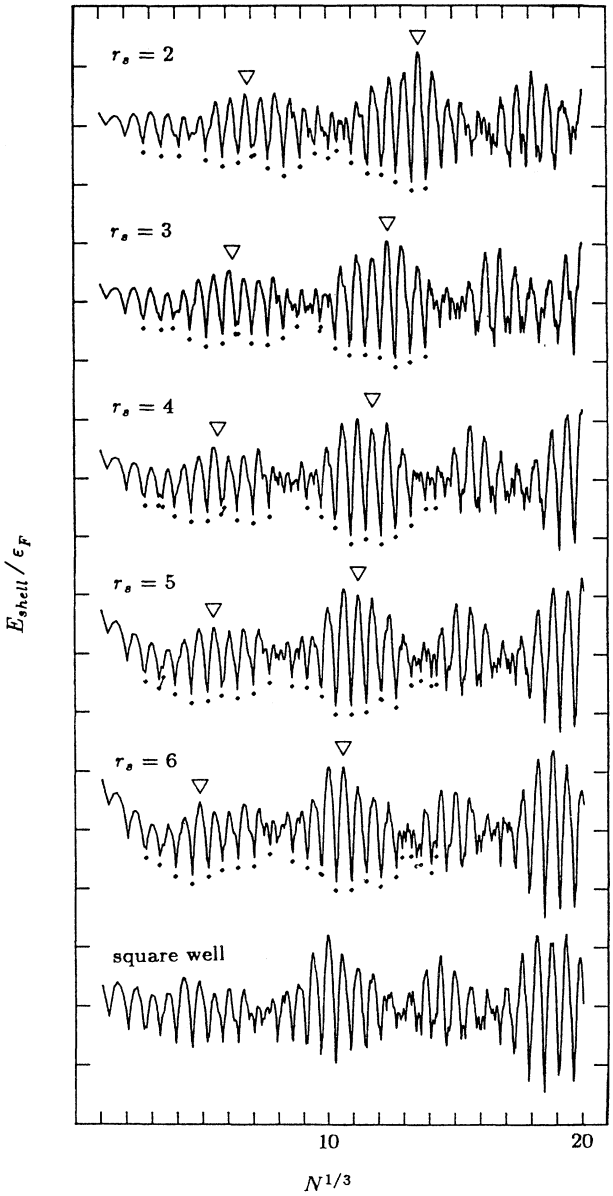

FIG. 2. $E_{\text{shell}}(N)$ as a function of $N^{1/3}$. The unit of energy is the Fermi energy ε_F. Dots mark N values listed in Table I as major supershell closings. Triangles mark "crossovers:" cluster sizes at which the highest l levels near the Fermi level become near degenerate ($a=3,4$).

TABLE I. Major supershell closings, $N < 3000$. Clusters with the number of valence electrons listed are identified with the closing of a supershell, with $E_{\text{shell}} < -\varepsilon_F/4$.

$r_s=2$	20, 40, 70, 138, 198, 268, 338–356, 440, 562, 706, 854, 1012, 1118, 1314, 1556, 1788, 2048, 2368, 2684
$r_s=3$	20, 40, 58, 92, 138, 198, 254–268, 338, 440, 556, 676, 912–926, 1100, 1284, 1516, 1760, 2048, 2334, 2672
$r_s=4$	20, 34–40, 58, 92, 138, 186–198, 254, 338, 440, 758, 912, 1074, 1284, 1502, 1760, 2018, 2328, 2654, 2886
$r_s=5$	20, 34–40, 58, 92, 138, 186, 254, 338, 440, 612, 748, 912, 1074, 1282, 1502, 1734–1760, 2018, 2314–2328, 2524, 2762, 2886
$r_s=6$	20, 34, 58, 92, 138, 186, 254, 338, 438, 612, 748, 890–912, 1074, 1282, 1502, 1734, 2018, 2130, 2314, 2420, 2524, 2762, 2886

cluded also for comparison.[23] The supershell pattern is similar in all cases. This similarity is directly related to the geometrical arguments of Ref. 12: so long as the surface width is much smaller than the cluster size, the closed classical orbits are approximately the same in dimensionless form for all metal clusters. The nodes do, however, shift substantially to smaller N with increasing r_s. Table I lists the values of N for which major supershell closings occur. The numbers at which these closings occur vary, but there is still a strong tendency for the same closing numbers to appear; especially for r_s values which are close, the sequences of numbers are similar.

The electron shells of a spherical cluster may be characterized by two quantum numbers: a radial quantum number v equal to the number of nodes in the radial wave function plus one, and the orbital angular momentum quantum number l. All states (v,l) have the $2(2l+1)$ degeneracy associated with orbital and spin angular momentum, but are otherwise mutually nondegenerate. In certain cases, however, near degeneracy can occur between two or more of these shells, which may then be considered a larger shell with the pseudoquantum number

$$\eta = av + bl \ , \tag{3.3}$$

where a and b are small integers.[24] The ratio $a:b$ of these integers describes the supershell pattern appropriate to a given case. We shall restrict our attention to the $a:1$ cases, as these correspond to the strongest effects.[12,13] In the special cases where the potential possesses some dynamical symmetry,[25] the appropriate pseudoquantum number may be an exact quantum number for all states: examples include the Coulomb potential ($a:b=1:1$) and the spherical harmonic-oscillator potential ($a:b=2:1$). In more general cases, the degeneracies will only be approximate. Appropriate ratios $a:b$ for metal cluster potentials vary, both with cluster size, and within a given cluster as a function of v and l. In the small cluster limit a 2:1 ratio gives a good description of level ordering: $\varepsilon(v,l) \simeq \varepsilon(v+1, l-2)$. As the cluster size increases, the ordering in energy of the higher angular momentum states gradually changes, causing near degeneracies $\varepsilon(v,l) \simeq \varepsilon(v+1, l-a)$ for $a=3,4,5,6,\ldots$ at the Fermi level over certain size ranges.

The size at which these near degeneracies occur may be characterized by identifying the smallest N for which $\varepsilon(1, l_{\max}) < \varepsilon(2, l_{\max}-a)$, where $l_{\max}$ is the state of highest angular momentum beneath the Fermi level. We shall refer to this condition as an $a:1$ "crossover." Calculations of the appropriate levels were extended to cluster sizes up to $N=66\,000$, to locate the values of N for which the $a:1$ crossovers ($a \leq 6$) would occur. These values of N are listed in Table II, and the 3:1 and 4:1 cases are indicated by triangles above the $E_{\text{shell}}(N)$ curves in Fig. 2. Major antinodes in the supershell structure are clearly associated with near-degeneracy of high angular momentum levels in a cluster.

B. Comparison with other work

The supershell effects calculated here are qualitatively very similar to those calculated in Ref. 13. The general pattern of nodes and antinodes, including their magnitude and their extent in N, is much the same. Overall, the closest correspondence with the Woods-Saxon potential calculation of Ref. 13 is found, not for $r_s=4$, but for $r_s=2$, where the Friedel oscillation effects are smallest.[26] As r_s increases, the deepening in the potential near the well edge gradually shifts the supershells toward the values found in the infinite square-well solution.

The distinctly different results obtained in this work for the various metallic densities are clearly reflected in experiment. For $r_s=2$, major features occur at $N=20,40,70,138,198$, in excellent agreement with recent experimental data for Al clusters.[6,27,28] Equally interesting is the absence of major features at $N=34,58,92$ both in the present calculation and in experiment. This is not necessarily an indication of a partial failure of the spherical jellium model, as has been recently suggested;[6] rather, the decrease of these features relative to $N=40,68-70$ is a natural tendency of shell models for metal clusters as the electron density increases.[29,30]

For $r_s=3$, experimental results are available for the noble metals Cu, Ag, and Au.[1,5] The abundance spectra of positive and negative Ag cluster ions show major features at $N=20,40,58,92,138,198$. The present calculation accurately exchanges the feature at $N=70$ in the $r_s=2$ case for features at $N=58,92$. The experimental results for

TABLE II. Values of N (and, in brackets, of $[l_{\max}]$) for which near-degeneracy occurs at the Fermi level for $a:b=3:1$, 4:1, 5:1, 6:1 shell structures in the spherical model.

r_s	3:1	4:1	5:1	6:1
2	320 [9]	2580 [21]	15 000 [41]	66 000 [70]
3	240 [8]	1930 [19]	12 000 [38]	53 000 [65]
4	180 [7]	1640 [18]	9 400 [35]	44 000 [61]
5	170 [7]	1400 [17]	8 000 [33]	36 000 [57]
6	120 [6]	1190 [16]	6 800 [31]	30 000 [54]

Cu and Au show similar features. More detailed comparisons of the spectra show differences between the shell patterns of Cu, Ag, and Au for the smallest clusters ($N \leq 40$) which cannot simply be described by changes in r_s;[1] for example, Au cluster ions have a feature at $N=34$ rather than at $N=40$. A more sophisticated treatment is required to describe these variations accurately. Nonetheless, we note that the observed variations from Cu to Ag to Au could be described by a progressive sharpening of the potential edge (as if, in the present calculation, r_s were allowed progressively to increase). Estimating the well depths U for each metal as the sum of the Fermi energy and the work function of the bulk metal, this progressive sharpening is just what is expected from the analysis of Sec. II; the surface thickness α becomes progressively smaller for Cu, Ag, and Au.

For the alkali metals, the present calculation gives an accurate description of all features of the shell structure seen in earlier studies ($N<100$), including the variation of shell structure with electronic density.[30,31] We also obtain excellent agreement with recent self-consistent spherical jellium calculations for Na ($r_s \simeq 4$) and Cs ($r_s \simeq 6$) for all major shell closings through $N=440$.[8-10] In particular, the shell closing at $N=40$ is present for Na, but absent for Cs. All calculations are in good agreement with experiment, although shell closings found in all calculations at $N=186$ and 254 are slightly lower in N than the corresponding experimental features. An explanation for this discrepancy may be found in the calculated ionization potential curve for Cs clusters.[8] In this calculation, a major shift in ionization energy, corresponding to a major energy gap, occurs at $N=186$ (as in the present work). The ionization energy continues to decrease slightly thereafter, however, reaching a local minimum around $N=198$; it is this local minimum which is reflected in experiment.

Only minor shell effects are observed experimentally between $N=440$ and 600 in Na and Cs clusters. This absence of major features appears to be associated with the first node in the supershell patterns in the present calculation. For Na, a very weak experimental feature[9] is observed at $N=558\pm 8$ which may correspond to a smaller feature at $N=556$ in the present calculation.

For Cs, the experimental feature at $N=557\pm 5$ remains unaccounted for, both in the present calculation and in a fully self-consistent one.[8] The present spherical model also fails in its description of features identified in abundance spectra of larger Na clusters ($700<N<1500$), and is clearly inadequate to describe the icosahedral or cuboctahedral structure observed in the largest Na clusters ($1500<N<22\,000$).[10] In the following section, we shall improve correspondence with experiment for $N<1500$ by including appropriate aspherical perturbations. Consideration of these aspherical effects will also lead to a simple description of the transition from spherical to protocrystalline shell structure.

IV. ASPHERICAL EFFECTS

Although spherical shell models have provided a simple, successful description of the basic features of metal clusters, many experimental results require an aspherical description: two examples are the plasma resonance splittings observed in small Na clusters[32] and the protocrystalline shells of atoms observed in large Na clusters.[10] We now consider to what extent these varied effects may be understood in the context of a general theory of aspherical perturbations.

Theoretical tools appropriate to the present problem have been developed in the study of collective effects in nuclei and crystal-field effects in ions.[18,33] We may expand the aspherical part of the one-particle potential in spherical harmonics[34]

$$V(r,\theta,\phi)=V_0(r)+\sum_{\lambda\geq 1}\sum_{\mu} v_{\lambda\mu}(r)Y^*_{\lambda\mu}(\theta,\phi)\ , \tag{4.1a}$$

imposing the constraint

$$v_{\lambda\mu}(r)=(-1)^{\mu}v^*_{\lambda-\mu}(r) \tag{4.1b}$$

to keep the potential real-valued. More detailed specification of the functional form of the $v_{\lambda\mu}(r)$ could be achieved, for example, by adopting the assumptions of the leptodermous model,[35] in which the variation of the potential is largely confined to a region near the surface. The results which follow, however, will not depend on these assumptions. The $\lambda=1$ terms in the expansion (4.1) correspond to a translation of coordinates in the leptodermous model, and are often omitted. The quadrupole and octupole terms ($\lambda=2,3$) are well known in nuclei, and have been considered for clusters.[36,37] Hexadecapole moments ($\lambda=4$) have also been identified in nuclei,[38] but these and higher moments are more common in the analysis of molecular spectra and crystal-field splittings of ions where octahedral or icosahedral symmetries are known to be involved.[33,39]

These examples illustrate two distinct mechanisms for aspherical deformation in metal clusters: spontaneous symmetry breaking and lattice effects. The spontaneous symmetry breaking with which we are concerned is independent of the lattice, and applies to any model in which spherical degeneracies of fermions occur. Lattice effects, on the other hand, are specifically associated with the fixed arrangement of the ionic cores. Opposed to these two mechanisms is the surface energy of the cluster, which increases with any variation away from spherical shape.

Order-of-magnitude estimates of the energy scales characteristic of each mechanism are instructive. A rough upper bound for the energy variation associated with symmetry breaking may be inferred from characteristic shell structure energies. For spherical shell structure to appear at all, the energy associated with symmetry breaking cannot be much greater than the part of the binding energy associated with spherical shell structure. Thus, following a discussion of shell effects in nuclei, we may write[40]

$$\Delta E(\text{symmetry breaking})\sim\pm\frac{3^{(2/3)}}{24}N^{1/3}\varepsilon_F$$
$$=\pm(0.09)N^{1/3}\varepsilon_F\ . \tag{4.2}$$

We consider the surface energy next. Variation of ΔS in

the surface area S causes a corresponding change in energy

$$\Delta E(\text{surface change}) \sim \frac{\Delta S}{S} a_s N^{2/3} \varepsilon_F = + \frac{\Delta S}{S} (0.18) N^{2/3} \varepsilon_F \ . \quad (4.3)$$

Here the numerical factor a_s is taken from the analytic value for the infinite square-well case (Appendix A); values from other sources are typically within a factor of 2 of this estimate. Geometric arguments for a volume-conserving shape variation from a sphere to a cuboctahedron give an estimate for the factor $(\Delta S/S)$ of 0.105. Finally, we estimate the energy variation for the change from a liquid state to an ordered lattice by taking the difference between liquid and crystalline values for the ion-ion interaction term in the theory of bulk metals.[41] We include in the estimate only the fraction $g(N_a)$ of atoms which, like their bulk counterparts, are full coordinated, i.e., atoms not on the surface:

$$\Delta E(\text{lattice ordering}) \simeq g(N_a) \frac{\hbar^2}{3m} (1.73 - 1.792) \times r_s^{-1} Z^{2/3} N = (-0.011) Z^{2/3} r_s N g(N_a) \varepsilon_F \ . \quad (4.4)$$

In this expression, Z is the valence of the metal, and $N_a = N/Z$ denotes the number of atoms in the cluster. The approach, which excludes the surface atoms entirely, and directly applies theories based on translational invariance of the interior atoms, is, of course, oversimplified. More sophisticated methods could be used, but this will suffice for the current discussion.

The different powers of N in Eqs. (4.2)–(4.4) make each of the three mechanisms important in different size ranges. In the small cluster limit, spontaneous symmetry breaking is the dominant effect, and quadrupole ($\lambda=2$) deformations arising from symmetry breaking must be included to give an accurate description of many observed effects.[32,36] As N increases, the energies associated with symmetry breaking and surface changes are both rapidly overtaken in magnitude by the lattice ordering energy; estimates for the relevant parameters suggest that lattice ordering should typically be the dominant effect above, say, 50 atoms. The argument is merely an order-of-magnitude estimate, but the physical significance remains clear: a transition (at $T=0$) is to be expected in this general size range from a liquidlike to a protocrystalline cluster. Detailed molecular-dynamics calculations of melting in free Au particles[42] substantiate this picture, and provide a more reliable quantitative estimate. In these calculations, no stable crystalline phase is found at $T=0$ for clusters with $N<200$, but cuboctahedra are found to be most stable for $N>200$. Experimentally, protocrystalline clusters of a few hundred atoms (both cuboctahedral and icosahedral) have been observed on substrates;[43] these results, however, must be interpreted with some care in the present context, since interactions with the substrate may strongly influence the crystallization.[44] The experimentally observed transition from electronic shell structure to shells of atoms in free Na clusters is in qualitative agreement with the present estimate, but occurs at a value of N which is over an order of magnitude larger.

To study this transition in more detail, we neglect spontaneous symmetry breaking and restrict our attention to the perturbation of valence-electron shells by a fixed protocrystalline lattice. For such a symmetric arrangement of atoms in a cluster, many of the $v_{\lambda\mu}(r)$ in (4.1) vanish. The analysis depends only on the rotational symmetry properties of the cluster; details are given in Appendix B. In particular, for clusters of octahedral or icosahedral symmetry, $v_{\lambda\mu}(r)=0$ for $\lambda=1,2,3$. The first nonzero terms in the expansion correspond to $\lambda=4$ for cuboctahedra, and $\lambda=6$ for icosahedra.

To apply perturbation methods, we assume the $v_{\lambda\mu}(r)$ to be small enough that the matrix elements $\langle \nu l j | \sum_{\lambda\mu} v_{\lambda\mu} Y^*_{\lambda\mu} | \nu' l' j' \rangle$ will generally be much smaller than the typical gap $\varepsilon_F N^{-1/3}$ between supershells. Here we have used the index j rather than the customary m to distinguish between the $2(2l+1)$ degenerate states of a given ν and l, to indicate that the unperturbed basis states we shall choose will not, in general, have orbital angular momentum that is quantized about an axis. Rather, we choose the sets of $2(2l+1)$ degenerate basis states $|\nu l j\rangle$ in such a way that the submatrix corresponding to the perturbation is diagonal, i.e., $\langle \nu l j | \sum_{\lambda\mu} v_{\lambda\mu} Y^*_{\lambda\mu} | \nu' l' j' \rangle = 0$ unless $j=j'$; we further assume that these nonzero diagonal elements are all different.[45] Given these assumptions, a perturbation treatment is valid.

For our purposes, the usefulness of the perturbation expansion lies in exploiting the symmetry of its terms, which result in vanishing matrix elements unless the conditions

$$l - l' - \lambda = \text{even} \ , \quad (4.5a)$$

$$|l - l'| \le \lambda \le l + l' \quad (4.5b)$$

are satisfied.[46] We begin by considering the first-order corrections

$$\varepsilon^{(1)}_{\nu l} = \langle \nu l | \sum_{\lambda\mu} v_{\lambda\mu} Y^*_{\lambda\mu} | \nu l \rangle \quad (4.6)$$

to the energy of the (ν,l) shell. The $\lambda=$odd terms in this expansion are zero by (4.5a); in particular, octupole distortions (whether spontaneous or fixed) will not affect the energy to first order. The $\lambda=$even terms will generally be nonzero, but we have assumed that they are small compared to the gap between supershells. Thus, if the $v_{\lambda\mu}$ are small enough that perturbation methods are applicable, the first-order energy corrections will not substantially alter the predictions of supershell structure obtained from a spherical model.

The second-order correction[45]

$$\varepsilon^{(2)}_{\nu l} = \sum_{\substack{\nu' l' j' \\ \nu l \neq \nu' l'}} \frac{\left| \left\langle \nu l j \left| \sum_{\lambda\mu} v_{\lambda\mu} Y^*_{\lambda\mu} \right| \nu' l' j' \right\rangle \right|^2}{\varepsilon(\nu,l) - \varepsilon(\nu',l')} \quad (4.7)$$

is a sum of terms which will be very small unless certain of the energy differences $\varepsilon(\nu,l) - \varepsilon(\nu',l')$ are smaller than

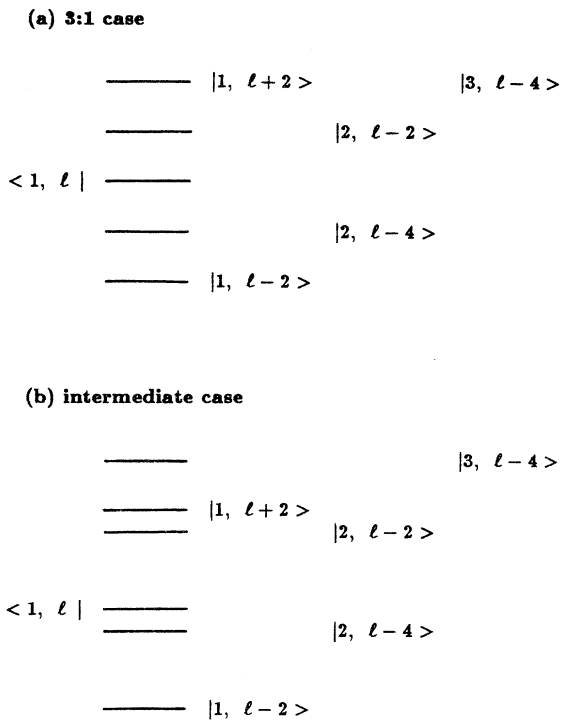

FIG. 3. Schematic energy-level diagrams detailing the terms which contribute to the sum (4.7) for (a) $a:b=3:1$, and (b) a case intermediate between 3:1 and 4:1. For discussion see text.

the corresponding matrix elements; that is, much smaller than the spacing between supershells. This, along with the restrictions (4.5), simplifies the problem considerably. We consider the case of a $Y^*_{4\mu}$ (cuboctahedral) perturbation. Figure 3 shows all nearby states which contribute to the sum (4.7) for the $(1,l)$ level in two different cases. States with $l'-l=$odd, or with $|l-l'|>4$, are omitted from the figure because the corresponding matrix elements are zero. In the 3:1 case [Fig. 3(a)], all remaining levels are far removed from the $(1,l)$ level, and the energy spacings are not small in comparison to the gap between supershells. Even the small level repulsion from the closest contributing levels $(2,l-2)$ and $(2,l-4)$ will roughly cancel, as they are approximately equally placed above and below the $(1,l)$ level. The second-order perturbation is thus negligible in the 3:1 case.

In the case intermediate between the 3:1 and 4:1 antinodes of the supershell pattern [Fig. 3(b)], the relative shift in energy levels results in the unperturbed $(2,l-4)$ level lying closer to the $(1,l)$ level. The decreasing energy denominator $\varepsilon(1,l)-\varepsilon(2,l-4)$ gradually causes the interaction between these levels to dominate the sum (4.7), and the resulting level repulsion pushes the $(1,l)$ level higher and the $(2,l-4)$ level lower. As the 4:1 crossover is approached, the energy denominator will decrease to the point that the second-order correction $\varepsilon^{(2)}_{\nu l}$ becomes comparable to the energy gap between supershells. At this point, the gap opened by the repulsion between these levels is the major experimental feature. Near the Fermi level, the $(1,l_{\max})$ level will be pushed upward into the next supershell. The revised supershell closings may then be calculated by subtracting the $2(2l_{\max}+1)$ electrons of the $(1,l_{\max})$ shell from the supershell closing numbers in the spherical theory, giving the alternate sequence of supershell closings in Table III. These are in much closer agreement with experiment than the results of the purely spherical model.

We may view this in another way. The level repulsion prior to the 4:1 crossover tends to move levels closer to the levels with which they were near-degenerate in the 3:1 case [Fig. 3(a)]. Thus the repulsion tends to stabilize the 3:1 supershell structure in this region, causing the supershells to remain roughly intact even when, in a purely spherical model, $\eta=3\nu+l$ can no longer be considered a good quantum number. This explains why the pseudoquantum number $\eta=3\nu+l$ is found[10] to apply to Na clusters over such a wide range in N.

Finally, at the cluster size for which the 4:1 crossover occurs, the energy difference essentially vanishes, and perturbation theory based on a spherical unperturbed potential is no longer valid. For this size region, even small shape distortions may result in large changes in level ordering, causing the supershell structure to disappear. In the presence of a $\lambda=4$ perturbation, the 3:1 supershell structure is stabilized to some degree, but the 4:1 structure is unstable. For metal clusters, where energy estimates suggest that the arrangement of the atomic cores can provide such a perturbation, the assumption that spherical effects are small breaks down entirely at this

TABLE III. Alternate supershell closings when a multipole perturbation with $\lambda=4$ is included. $N_{\rm sph}$ are the shell closings in the spherical shell theory, $N_{\rm pert}$ the revised shell closings when the perturbation is applied, and $N_{\rm expt}$ the experimental values.

$l_{\max}$	$N_{\rm sph}$	$2(2l_{\max}+1)$	$N_{\rm pert}$	$N_{\rm expt}$(Cs)[a]	$N_{\rm expt}$(Na)[b]
12	612	50	562	557 ±5	
13	758	54	704		700 ±15
14	912	58	854		840 ±15
15	1074	62	1012		1040±20
16	1284	66	1218		1220±20
17	1502	70	1432		1430±20

[a]Reference 8.
[b]Reference 10.

point. This is not a spontaneous symmetry breaking effect; it involves the atomic lattice, which reaches a substantially lower energy by becoming ordered in this way. As clusters grow even larger, the energy balance becomes still more strongly in favor of such protocrystalline configurations. Moreover, near degeneracy persists between certain (ν,l) and $(\nu+1,l-4)$ levels, occurring at energies gradually deeper in the well, below the Fermi energy. The breakdown of the spherical model is therefore not limited merely to the size at which the 4:1 crossover occurs, but persists thereafter as well.

The preceding arguments are essentially the same for a $Y^*_{6\mu}$ (icosahedral) perturbation, except that $(\nu,l\pm6)$ levels must also be included in Fig. 3. At the 3:1 crossover, a $(3,l-6)$ state would then be near-degenerate with the $(1,l)$ state, and these would, in general, be coupled by a nonzero matrix element. If icosahedral crystalline structure were favored energetically for sizes smaller than the size for which the 3:1 crossover occurs, then a breakdown of the spherical approximation would occur for a $Y^*_{6\mu}$ perturbation at this point. Such an effect has not yet been observed experimentally. The lattice ordering energy per atom increases with the valency of the metal, varying as $Z^{5/3}$; the tetravalent[7] metal Pb is therefore a potential candidate for such an effect. Apart from this difference, the $Y^*_{6\mu}$ case follows the same lines as the preceding discussion. In particular, in the 4:1 crossover region the argument proceeds just as in the $Y^*_{4\mu}$ case, with the same result: the perturbation theory breaks down, and spherical supershell structure is eradicated.

The present argument has deliberately been kept as general as possible, based largely on symmetry considerations. Despite the generality of the argument, in conjunction with the calculations of Sec. III it leads to a very quantitative result. For metal clusters which can be modeled by a spherical mean-field potential, and for which the above perturbation treatment is valid, the number of electrons N corresponding to the 4:1 crossover at the Fermi level characterizes the size at which a transition occurs from spherical to protocrystalline shell structure. For Na, this crossover is found in the present work to occur at $N=1640$, in excellent agreement with the experimentally observed change from spherical electronic shell structure to shells of atoms in the region $1400<N<2000$.[10]

Three final comments are in order. First, it does not follow that clusters have no ordering of ionic cores until the 4:1 crossover. On the contrary, the success of the aspherical perturbation treatment presented here for $500<N<1500$ indicates that significant protocrystalline structure is already present prior to the crossover. Rather, the 4:1 crossover marks the point at which protocrystalline structure is reflected in the energy-level distribution. This distinction is useful in understanding the order-of-magnitude discrepancy between the estimates of cluster crystallization and the size at which a transition to shells of atoms is observed experimentally in abundance spectra. Protocrystalline ordering of the ionic cores may occur for clusters of a few hundred atoms or less, but their effect on the energy-level distribution is minor until the 4:1 crossover is reached.

Second, the argument presented here neglects finite-temperature effects, and therefore strictly applies only in the $T=0$ limit. Indeed, recent experiments on large Na clusters[47] in which the cluster temperature is deliberately kept high ($T\sim100\,^\circ$C–$200\,^\circ$C) continue to display features characteristic of electronic shell structure up to $N=2700$.

Third, the present results suggest another approach to the morphology of free metal clusters in this size range. A cuboctahedral packing of shells of atoms differs from an icosahedral packing merely by a small stretching and shrinking along suitable axes.[48] The energy barrier between cuboctahedral and icosahedral configurations should therefore be very small; indeed, single particles on substrates have been observed to fluctuate between the two configurations under electron irradiation.[43] We conjecture that the spherical shell structure of the valence electrons of a metal cluster may in some cases determine which aspherical configuration has lowest energy. An a:1 shell structure has associated with it multipole deformations of order $\lambda=a,2a,3a,\ldots$.[49] Based on the decomposition into spherical harmonics of cuboctahedral ($\lambda=4,6,8,9,10,\ldots$) and icosahedral ($\lambda=6,10,\ldots$) shapes (Appendix B), we conjecture that a 4:1 shell structure will favor cuboctahedral shapes.

V. SUMMARY

Calculations of supershell structure in metal clusters have been presented over the entire range of metallic densities. Good agreement is obtained with detailed variations in experimental data for metal clusters ranging from Al ($r_s\simeq2$) to Cs ($r_s\simeq6$), and with corresponding self-consistent jellium calculations. The model is based on self-consistent potentials for the bulk metal surface, but requires far less computational effort than fully self-consistent calculations for each cluster; this should make it especially useful for surveys of properties of clusters over a wide range in N, and for studies of the larger clusters.

Examination of the details of spherical supershells in metal clusters has led to an explanation for the recently observed transition to shells of atoms in Na clusters. The present analysis suggests that the $T=0$ transition to an energy-level distribution characteristic of polyhedra rather than spherical shells will occur for any simple free-electron metal at a cluster size corresponding to near-degeneracy at the Fermi level between valence-electron states differing by $\Delta l=4$. This condition is fulfilled by clusters with on the order of $N\sim10^3$ valence electrons for all metallic densities. For N smaller than the critical

TABLE IV. Coefficients of the four-parameter least-squares fit (3.2) $E_{\rm av}(N)$ for various values of r_s.

r_s	a_v	a_s	a_c	a_d
2	0.599 224	0.325 55	0.1772	−0.407
3	0.599 075	0.231 75	0.5165	−0.658
4	0.599 364	0.119 41	0.9263	−1.086
5	0.599 969	0.045 01	1.2730	−1.560
6	0.600 346	−0.035 92	1.5077	−1.807

value, the perturbations from the incipent ionic lattice actually stabilize the supershell structure of the electronic levels, causing the supershell model to apply over a larger range in N than might have been expected from energy balance arguments alone.

ACKNOWLEDGMENTS

I am pleased to record my thanks to W. D. Knight for continued encouragement, stimulating correspondence, and a careful reading of the manuscript; to J. Dong, W. Jiang, and J. F. Zhang for assistance with computers; and to K. Q. Lu, S. S. Xie, and B. Y. Gu for use of their computer facilities, discussions, and support. The ongoing assistance and support of G. Z. Yang and K. H. Zhao are gratefully acknowledged. This work was supported by the Natural Science Foundation of China.

APPENDIX A: LIQUID-DROP MODEL

We present here details of the parametrized fit $E_{\rm av}(N)$ to the total energy $E(N)$. The numerical values found for the coefficients of the four-parameter fit (3.2) are displayed in Table IV. This fit provides an excellent smoothed curve for isolation of shell effects, but if a_s and a_c are interpreted as the surface and curvature energy coefficients in analogy with a liquid-drop model, the surface energy becomes negative for $r_s=6$. Therefore a least-squares fit was also performed for the three-parameter fit

$$E_{\rm av}(N)=\varepsilon_F(a_v N+a_s N^{2/3}+a_c N^{1/3}) . \tag{A1}$$

The resulting coefficients are listed in Table V. The curvature energy in this case is found to be negligible, and the surface energies are all positive. These coefficients are expected to provide better estimates of the surface energy of a cluster than those listed in Table IV, though the lack of self-consistency in the present calculations may seriously affect the surface energy.

As a further check on the calculation, we present an analytic solution for a_v and a_s for the infinite spherical square well of radius R_0. In this special case, we may use the expression (2.4) for the density of eigenvalues with Dirichlet boundary conditions to evaluate the integrals

$$E_{\rm total}=\int_0^{k_F}\rho(k)E(k)dk , \tag{A2}$$

$$E(k)=\varepsilon_F(k/k_F)^2 , \tag{A3}$$

$$N=\int_0^{k_F}\rho(k)dk , \tag{A4}$$

for total energy $E_{\rm total}$ and number N of valence electrons in the well. Expanding the quotient of these two integrals in powers of $(S/\Omega k_F)$, we have

$$\frac{E_{\rm total}}{N}=\varepsilon_F\left[\frac{3}{5}+\frac{3\pi}{80}\left[\frac{S}{\Omega k_F}\right]+\cdots\right] , \tag{A5}$$

TABLE V. Coefficients of the three-parameter least-squares fit (A1) $E_{\rm av}(N)$ for various values of r_s.

r_s	a_v	a_s	a_c
2	0.598 656	0.344 41	−0.0004
3	0.596 977	0.296 40	−0.0025
4	0.595 527	0.237 03	−0.0048
5	0.594 754	0.205 40	−0.0064
6	0.594 124	0.154 98	−0.0077

where the surface term arises from the difference of two considerably larger terms, and is thus very sensitive to changes in boundary conditions. For a sphere of radius R_0,

$$\frac{S}{\Omega k_F}=\left[\frac{12}{N\pi}\right]^{1/3} , \tag{A6}$$

and a_v and a_s are determined by equating coefficients of corresponding powers of N in (A1) and (A5). We find

$$a_v=\tfrac{3}{5}=0.6 ,$$

$$a_s=\frac{1}{20}\left[\frac{9\pi}{4}\right]^{2/3}=0.184 . \tag{A7}$$

The value for a_s derived in this way corresponds exactly to analytic estimates of surface energy per unit area in the theory of liquid metals.[50] In view of the sensitive variation of a_s with boundary conditions, the correspondence of these idealized coefficients with the values for the three-parameter fit is acceptable.

APPENDIX B: SYMMETRY RESTRICTIONS ON TERMS IN THE ASPHERICAL POTENTIAL

If we neglect spontaneous symmetry breaking and consider a symmetric arrangement of atoms in a cluster, many of the $v_{\lambda\mu}$ in (4.1) are identically zero. This may be demonstrated using group theory. We consider the group of rotations which leaves the potential V of an aspherical cluster (here a cuboctahedron, or an icosahedron) invariant. This group is a subset of the group of all rotations; and the representation D_λ of the group of all rotations is in general reducible for this smaller group. This reduction or decomposition of the D_λ is straightforward,[51] and resulting sets of irreducible representations are available in the literature for the octahedral[52] and icosahedral[53] groups. If these sets of irreducible representations of the octahedral (icosahedral) group do not contain the unit representation for a given $\lambda=L$, then no linear combination of the $Y^*_{L\mu}$ exists that maintains the complete potential V invariant under every rotation of the given group. If the potential is to have the desired symmetry, then, we must fix $v_{L\mu}=0$. We reproduce here the sequence of λ values ($\lambda\le 10$) for which the coefficients $v_{\lambda\mu}$ may be nonzero: For octahedral symmetry; $\lambda=0,4,6,8,9,10$; for icosahedral symmetry, $\lambda=0,6,10$.

*Permanent address: U.S. National Academy of Sciences, Beijing Office, Friendship Hotel Room 40522, Beijing 100873, People's Republic of China.

[1]W. A. de Heer, W. D. Knight, M. Y. Chou, and M. L. Cohen, in *Solid State Physics*, edited by H. Ehrenreich and D. Turnbull (Academic, New York, 1987), Vol. 40, p. 93.

[2]Proceedings of the Fourth International Meeting on Small Particles and Inorganic Clusters, Aix-en-Provence, 1988 [Z.

Phys. D **12** (1989)].
[3]M. L. Cohen and W. D. Knight, Phys. Today **43** (12), 42 (1990).
[4]W. D. Knight, K. Clemenger, W. A. de Heer, W. A. Saunders, M. Y. Chou, and M. L. Cohen, Phys. Rev. Lett. **52**, 2141 (1984).
[5]I. Katakuse, T. Ichihara, Y. Fujita, T. Matsuo, T. Sakurai, and H. Matsuda, Int. J. Mass Spectrom. Ion Proc. **67**, 229 (1985); **69**, 109 (1986); **74**, 33 (1986).
[6]K. E. Schriver, J. L. Persson, E. C. Honea, and R. L. Whetten, Phys. Rev. Lett. **64**, 2539 (1990).
[7]I. Rabin, W. Schulze, and B. Winter, Phys. Rev. B **40**, 10 282 (1989).
[8]H. Göhlich, T. Lange, T. Bergmann, and T. P. Martin, Phys. Rev. Lett. **65**, 748 (1990).
[9]S. Bjørnholm, J. Borggreen, O. Echt, K. Hansen, J. Pedersen, and H. D. Rasmussen, Phys. Rev. Lett. **65**, 1627 (1990).
[10]T. P. Martin, T. Bergmann, H. Göhlich, and T. Lange, Chem. Phys. Lett. **172**, 209 (1990).
[11]R. Balian and C. Bloch, Ann. Phys. **60**, 401 (1970).
[12]R. Balian and C. Bloch, Ann. Phys. **69**, 76 (1972).
[13]H. Nishioka, K. Hansen, and B. R. Mottelson, Phys. Rev. B **42**, 9377 (1990).
[14]N. D. Lang and W. Kohn, Phys. Rev. B **1**, 4555 (1970).
[15]We make the common assumption that the bulk density may be applied to clusters of all sizes: see, for exmaple, D. R. Snider and R. S. Sorbello, Phys. Rev. B **28**, 5702 (1983); L. B. Hansen, P. Stoltze, J. K. Nørskov, B. S. Clausen, and W. Niemann, Phys. Rev. Lett. **64**, 3155 (1990).
[16]The relative insensitivity of bound-state calculations to the choice of the well depth is illustrated by the successful description of many bound-state properties by Thomas-Fermi theory [V. Kresin, Phys. Rev. B **38**, 3741 (1988)], in which the well depth is ε_F for all densities.
[17]The line of argument here extends a method of estimation presented in A. deShalit and H. Feshbach, *Theoretical Nuclear Physics* (Wiley, New York, 1974), Vol. 1, pp. 128–130. The factor $\pi/2$ in their equation (3.10) is $\pi/4$ in the more rigorous expression of Balian and Bloch (Ref. 11).
[18]A. Bohr and B. R. Mottelson, *Nuclear Structure* (Benjamin, Reading, MA, 1969), Vol. I, pp. 140ff; *Nuclear Structure* (Benjamin, Reading, MA, 1975), Vol. II, p. 589.
[19]D. E. Beck, Phys. Rev. B **30**, 6935 (1984).
[20]W. Ekardt, Phys. Rev B **29**, 1558 (1984).
[21]This corresponds to $v_{\text{eff}} = -1.0000$ in the units of Ref. 14.
[22]The term $(l+\frac{1}{2})^2$ was used to approximate the $l(l+1)$ term in the centrifugal potential; for a full discussion, see N. Fröman and P. O. Fröman, *JWKB Approximation: Contributions to the Theory* (North-Holland, Amsterdam, 1965).
[23]This calculation was performed numerically using the same WKB approximation method with square-well potentials for each N of radius R_0.
[24]A. Bohr and B. R. Mottelson, *Nuclear Structure* (Ref. 18), Vol. II, pp. 579ff.
[25]For example, see L. I. Schiff, *Quantum Mechanics,* 3rd ed. (McGraw-Hill, New York, 1968), p. 234ff.
[26]For the smallest clusters, the supershell closings of Ref. 13 do correspond with the $r_s = 4$ calculation. This variation appears to be associated with the use of a different radius parameter to model spillout at the cluster surface.
[27]R. E. Leuchtner, A. C. Harms, and A. W. Castleman, Jr., J. Chem. Phys. **94**, 1093 (1991).
[28]M. F. Jarrold, J. E. Bower, and J. S. Krauss, J. Chem. Phys. **86**, 3876 (1987).
[29]The results differ somewhat from those of a self-consistent jellium calculation [M. Y. Chou and M. L. Cohen, Phys. Lett. **113A**, 420 (1986)] in which significant features are also predicted near $N = 58, 92$. In the present calculation, the shell closings associated with these numbers of electrons are minor.
[30]A discussion of the trends in the relative size of shell closing gaps with r_s is given by M. Y. Chou, A. Cleland, and M. L. Cohen, Solid State Commun. **52**, 645 (1984).
[31]W. D. Knight, W. A. de Heer, K. Clemenger, and W. A. Saunders, Solid State Commun. **53**, 445 (1985).
[32]K. Selby, V. Kresin, J. Masui, M. Vollmer, W. A. de Heer, A. Scheidemann, and W. D. Knight, Phys. Rev. B **43**, 4565 (1991).
[33]J. S. Griffith, *The Theory of Transition-Metal Ions* (Cambridge University, London, 1961).
[34]A discussion of the motivation for, and the limits of, such an expansion may be found in Ref. 33, pp. 195–202. Our form is somewhat more general than Griffith's, as we do not assume $r < R$ (Ref. 83, p. 202, example 3). Equation (4.1b) assumes the Condon-Shortley phase convention.
[35]A. Bohr and B. R. Mottelson, *Nuclear Structure* (Ref. 18), Vol. II, pp. 137–139.
[36]K. Clemenger, Phys. Rev. B **32**, 1359 (1985).
[37]I. Hamamoto, B. Mottelson, H.-X. Xie, and X.-Z. Zhang (unpublished).
[38]D. L. Hendrie *et al.,* Phys. Lett. **26B**, 127 (1968).
[39]W. G. Harter, in *XV International Colloquium on Group Theoretical Methods in Physics,* edited by R. Gilmore (World Scientific, Singapore, 1987), p. 1.
[40]A. Bohr and B. R. Mottelson, *Nuclear Structure* (Ref. 18), Vol. II, p. 599. In this expression, we have substituted $\hbar\omega_0 = \varepsilon_F N^{-1/3}$; cf. Ref. 1, p. 173.
[41]N. W. Ashcroft and D. C. Langreth, Phys. Rev. **155**, 682 (1968), and references cited therein.
[42]F. Ercolessi, W. Andreoni, and E. Tosatti, Phys. Rev. Lett. **66**, 911 (1991).
[43]S. Iijima and T. Ichihashi, Phys. Rev. Lett. **56**, 616 (1986).
[44]P. M. Ajayan and L. D. Marks, Phys. Rev. Lett. **63**, 279 (1989).
[45]E. U. Condon and G. H. Shortley, *The Theory of Atomic Spectra* (Cambridge University, London, 1935), pp. 30–37. Both v and l in this paper correspond to their index n, as both count states distinct in energy; the index j corresponds to their index l, as it counts states which are degenerate.
[46]See, for example, A. Messiah, *Quantum Mechanics* (North-Holland, Amsterdam, 1961–62), Appendix C.
[47]J. Pedersen *et al.* (unpublished).
[48]A. L. Mackay, Acta Crystallogr. **15**, 916 (1962).
[49]A. Bohr and B. R. Mottelson, *Nuclear Structure* (Ref. 18), Vol. II, p. 591.
[50]C. A. Croxton, *Statistical Mechanics of the Liquid Surface* (Wiley, New York, 1980), p. 150.
[51]See, for example, M. Tinkham, *Group Theory and Quantum Mechanics* (McGraw-Hill, New York, 1964), p. 70.
[52]S. L. Altmann and A. P. Cracknell, Rev. Mod. Phys. **37**, 19 (1965).
[53]N. V. Cohan, Proc. Cambridge Phil. Soc. Math. Phys. Sci. **24**, 28 (1958).